Spatial Extent of New Particle Formation Events over the Mediterranean basin from multiple ground-based and airborne measurements

Kevin Berland[1], Clémence Rose[1], Jorge Pey[2], Anais Culot[1], Evelyn Freney[1], Nikolaos Kalivitis[3], Giorgios Kouvarakis[3], José Carlos Cerro[4], Marc Mallet[8], Karine Sartelet[6], Matthias Beckmann[7], Thierry Bourriane[8], Greg Roberts[8], Nicolas Marchand[2] Nikolaos Mihalopoulos[3,9] and Karine Sellegri[1]

[1]Laboratoire de Météorologie Physique, CNRS UMR 6016, Université Blaise Pascal, Aubière, France

[2]Aix-Marseille Université, CNRS, LCE, UMR 7376, 13331, Marseille, France

[3]Environmental Chemical Processes Laboratory, University of Crete, Heraklion, Crete, 71003, Greece

[4]Laboratory of Environmental Analytical Chemistry, Illes Balears University, Palma, 07122, Spain

[5]Laboratoire d'Aérologie (LA), Université de Toulouse, CNRS, Toulouse, France

[6]CEREA, joint laboratory Ecole des Ponts ParisTech - EDF R&D, Université Paris-Est, 77455 Champs sur Marne, France.

[7]Laboratoire Interuniversitaire des Systèmes Atmosphériques (LISA), UMR-CNRS 7583, Université Paris-Est-Créteil (UPEC) et Université Paris Diderot (UPD), Institut Pierre Simon Laplace (IPSL), Créteil, France

[8]Centre National de Recherches Météorologiques, Météo-France, Toulouse, URA1357, France

[9]IERSD, National Observatory of Athens, P. Penteli, 15236, Athens, Greece

Correspondence to: Karine Sellegri (K.Sellegri@opgc.cnrs.fr)

Abstract. Over the last two decades, new particle formation (NPF), i.e. the formation of new particle clusters from gas-phase compounds followed by their growth to the 10-50 nm size range, has been extensively observed in the atmosphere at a given location, but their spatial extent rarely assessed. In this work, we use aerosol size distribution measurements performed simultaneously at Ersa (Corsica) and Finokalia (Crete) over a one-year period to analyze the occurrence of NPF events in the Mediterranean area. The geographical location of these two sites, as well as the extended sampling period allow us to assess the spatial and temporal variability of atmospheric nucleation at a regional scale. Finokalia and Ersa show similar seasonalities in the monthly average nucleation frequencies, growth rates, and nucleation rates although the two stations are located more than 1000 km away from each other. Within this extended period, aerosol size distribution measurements were performed during an intensive campaign (July 3rd to August 12th 2013) from a ground based station on the island of Mallorca, as well as onboard the ATR-42 research aircraft. This unique combination of stationary and mobile measurements provides us with detailed insights into the horizontal and vertical development of the NPF process on a daily scale. During the intensive campaign, nucleation events occurred simultaneously both at Ersa and Mallorca over delimited time slots of several days, but different features were observed at Finokalia. The results highlight that the spatial extent of the NPF events over the Mediterranean Sea might be as large as several hundreds of kilometers, mainly determined by synoptic conditions. Airborne measurements gave additional information regarding the origin of the clusters detected above the sea. The selected cases depicted contrasting

situations, with clusters formed in the marine boundary layer or initially nucleated above the continent or in the free troposphere (FT) and further transported above the sea.

1 Introduction

New particle formation (NPF) events have been widely observed in the atmosphere in different environments (Kulmala et al., 2004) from remote areas at high altitude or latitude to polluted environments in different climates (Pey et al., 2008; Manninen et al., 2010; Yli-Juuti et al., 2011; Cusack et al., 2013). However, the exact mechanism and chemical species involved in the NPF process are not fully identified, especially regarding the diversity of environments to consider. Thus, most global climate models still do not represent well this process, and use parameterizations which are based upon a limited number of mechanisms and gaseous precursors, even though they predict that it may contribute to a significant fraction of condensation nuclei (CN) and cloud condensation nuclei (CCN) concentration at the global scale (Spracklen et al., 2008; Merikanto et al., 2009; Makkonen et al., 2012).

The different features of NPF events (frequency, intensity, duration) may be influenced by meteorological variables (temperature, relative humidity and solar radiation) (Birmili et al., 2003; Jeong et al., 2004; Sihto et al., 2006; Young et al., 2007), but also by the availability of gaseous precursors, regarding both their nature and their amount. It is thus necessary to describe the occurrence and characteristics of NPF over a large variety of environments, and assess to what spatial extent these features can be applied to. Although the characteristics of the NPF events have often been documented in the literature (Hirsikko et al., 2007; Manninen et al., 2010; Yli-Juuti et al., 2009, 2011), analysis dedicated to their spatial extent are rarer. This might be explained by the fact that such studies require airborne measurements (Crumeyrolle et al. 2010; Rose et al., 2015a) or multi-sites datasets. Such datasets were analyzed by Vana et al. (2004) and Hussein et al. (2009) who reported that NPF could take place in the form of regional events over up to a thousand kilometers in Scandinavia, and at least 500 kilometers over the western coast of Korea (Kim et al. 2016). Likewise, Dall'Osto et al. (2013) observed regional NPF events occurring in the north-east of Spain. Using a similar methodology, Crippa and Pryor, (2013) observed horizontal extents of a hundred kilometers for the NPF process in USA and Canada. They also pointed out a significant variability of the NPF characteristics (formation and growth rates) within these large-scale events, suggesting that local signatures could superimpose to favorable synoptic conditions. In order to allow for the analysis of the horizontal extent of NPF on a single station dataset, different methods based on air mass back trajectory analysis and particle growth rates were also recently proposed (Kristensson et al., 2014; Rose et al., 2015b). The Nanomap tool developed by Kristensson et al., (2014) was reported to allow the identification of nucleation areas up to 500 km away from the observation site. The main limitation of this last method is due to the fact that the determination of the nucleation area directly depends on event characteristics that sometimes cannot be accurately defined (i.e. the determination of the end of the nucleation process itself, or the end of the growth process).

These studies dedicated to the analysis of the horizontal extent of NPF were mainly conducted above continental regions. Similar analysis in marine environments are crucially missing although they are of high interest, as it was previously shown that in such pristine environments, cloud properties could be significantly impacted by changes in the aerosol loading (Tao et al., 2012; Koren et al., 2014; Rosenfeld et al., 2014). Although the

Mediterranean area is particularly sensitive to the future evolution of atmospheric pollutants and climate change, only a few studies related to NPF in this area have been reported so far. Intensive campaigns were conducted on the eastern Spanish coast, in Barcelona and at Montseny site (Pey et al., 2008; Cusack et al., 2013), while long-term measurements are performed at the Finokalia (Crete) station (Kalivitis et al., 2008, 2012, 2015; Manninen et al., 2010; Pikridas et al., 2012), where NPF event days are close to 30%. The Mediterranean basin is at the cross section of many different influences: there is a strong anthropogenic influence from densely populated coastal zones, which superimpose with marine and dust sources, as well as with emissions from Mediterranean forests and shrublands that emit both terpenes and isoprene. This geographical area is particularly exposed to high solar radiation compared to the rest of Europe, so that we expect a strong contribution from photochemical processes.

In the framework of the projects CHARMEX-ADRIMED (Mallet et al., 2015) and CHARMEX-SafMed, a large coordinated effort has been recently conducted to better characterize the physico-chemical properties of the Mediterranean atmosphere. Measurements were conducted at ground-stations on Mediterranean islands, such as Crete (Finokalia) and Corsica (Ersa) for an extended period of the years 2013-2014 and Mallorca (Cap Es Pinar) for several weeks during 2013. Forty research flights were also performed during the summers 2013 and 2014. This vast dataset gave us a unique opportunity to characterize the spatial extent of the NPF process in the Mediterranean basin. In this paper, we first report the long-term analysis of NPF event characteristics observed at Ersa (from May 2012 to August 2013) and Finokalia (from January to December 2013) using size distribution measurements in order to assess the large-scale space and time variability of NPF. We then focus our study on the Special Operation Period (SOP) that took place during summer 2013. During this SOP additional measurements were performed in Mallorca (from July 3rd to August 12th 2013) and aerosol particle size distributions and concentrations were measured onboard the ATR-42, which allowed for a deeper analysis of the horizontal and vertical development of the NPF process at daily scale.

2 Experimental platforms, material and methods

2.1 Ground-based measurements

Ground-based aerosol measurements reported in this work were performed at the Finokalia station (Crete) from January to December 2013, at the Ersa station (Corsica) from May 2012 to August 2013, and at the Cap Es Pinar station (Mallorca) from July 3rd to August 12th 2013 (Fig. 1). Within these measurements periods, some gaps occurred in the Finokalia dataset (from September 5th to October 15th 2013) due to participation of the instrument in the ACTRIS (Aerosol Clouds and Trace gases Research Infrastructure) network mobility particle size spectrometer workshop, and in the Ersa dataset (from September 1st to October 31th 2012) because of instrumental failures.

The Finokalia station (35.24° N, 25.60° E) is located on the northern coast of Crete, Greece, at the top of a hill (230 m a.s.l) facing the sea. There is no significant human activity within an area of approximately 15 km around the station, mainly characterized by a scarce vegetation (Mihalopoulos et al., 1997). The closest large urban area is the city of Heraklion, with 150 000 inhabitants, located 50 km west from Finokalia. Aerosols at the site are mainly transported from the south-eastern Europe and northern Africa, and to a lesser extent from central and

western Europe (Kouvarakis et al., 2000; Sciare et al., 2008; Pikridas et al., 2010, 2012). At Finokalia, aerosol particle size distributions were measured in the size range 9 - 849 nm with a time resolution of 300 s with a custom-made scanning mobility particle sizer (SMPS) (Wiedensohler et al., 2012). As previously described by Kalivitis et al., (2015), the system operates with a closed-loop sheath air flow with a 5:1 ratio between the sheath and the aerosol flow. It comprises a Kr-85 aerosol neutralizer (TSI 3077), a Hauke medium differential mobility analyzer (DMA) and a TSI-3772 condensation particle counter (CPC). The system is operated following the recommendations of Wiedensohler et al., (2012), thus meeting the European infrastructure ACTRIS project requirements for quality insurance.

The Ersa station is located on the northern tip of Corsica Island, on Cape Corsica (43.00° N, 9.30° E, 530 m a.s.l.). On this part of the island the wind can be very strong with frequent windstorms (78 days in 2007 with wind speeds stronger than 28 m s^{-1}). Climate in Corsica is characterized by moist winters and dry summers, with less than 100 rainy days per year (Lambert et al., 2009). Aerosols reaching the site are of variable types, including mineral dust particles from north Africa, anthropogenic and biomass burning aerosols mainly originating from densely populated coastal areas located in eastern Spain, France and Italy, and marine aerosols, from the Mediterranean Sea itself but also from the Atlantic Ocean (Nabat et al., 2013; Mallet et al., 2016). The Cape Corsica peninsula is a remote site, excluding important local anthropogenic sources that could affect the in-situ measurements, and surrounded by a scarce Mediterranean vegetation (Mallet et al., 2016). At Ersa, aerosol size distributions were measured with a scanning mobility particle sizer (SMPS TSI 3080, associated to a CPC TSI 3010) in the size range 10 - 495 nm with a time resolution of 300 s.

The Cap Es Pinar station is located on the northeastern side of the Mallorca Island (39.88° N, 3.19° E, 20 m a.s.l.), on a peninsula between the Alcudia and Pollença bays. The station was established in one of the buildings belonging to the Spanish Ministry of Defense in its Cap Es Pinar facilities. The area is densely forested by Mediterranean shrublands and pine trees and the access to the station is restricted. Urban centers, the Alcudia and Pollença harbors and main roads are located at least 10 km from the site. Particle size distributions were measured in the size range 15-600 nm with a time resolution of 300 s using a TSI SMPS, with a 3081 long DMA and a CPC TSI 3776.

2.2 Airborne measurements

Airborne measurements were carried out onboard the ATR-42 French research aircraft operated by SAFIRE (Service des Avions Français Instrumentés pour la Recherche en Environnement). Figure 1 shows the aircraft trajectory during the flights performed on July 30th and August 1st which are investigated in the next sections of the present work. The aerosol size distribution in the 20-485 nm diameter range was measured with a time resolution of 130 s using the SMPS system previously described in Crumeyrolle et al. (2010) which includes a CPC TSI 3010, a differential mobility analyser (DMA) and a krypton aerosol neutralizer. The total concentrations of aerosols larger than 10 nm (N_{10}) and larger than 3 nm (N_3) were measured using a custom-made CPC dedicated to aircraft measurements (Weigel et al., 2009) and a CPC TSI 3025, respectively. The concentration of particles in the size range 3 - 10nm (N_{3-10}) was calculated as the difference between N_3 and N_{10}. After analysis of the variability of N_{3-10} apart from nucleation periods, we found that N_{3-10} concentrations are above the variability of the two CPC concentration difference when exceeding the threshold of 395 cm^{-3}. For

more details on the airborne instrumentation and data analysis procedure, the reader is referred to Rose et al., (2015a).

3 Data analysis

3.1 NPF events classification

From ground-based observations, measurement days were classified according to Dal Maso et al. (2005) into four categories: events days, including classes I and II, undefined and non-events days. Class I events are characterized by a strong increase of sub-25nm particles concentrations, their persistence over a period of more than an hour and a clear growth of the nucleation mode particles towards larger sizes during the following hours. Class II events have the same characteristics as Class I events, except that they may be less intense or show a discontinuity in the growth of the clusters. Days are considered undefined when the newly observed particles are detected only from the Aitken size and/or when they do not grow during the course of the day.

3.2 Particle formation and growth rates calculations

Particle formation and growth rates are key entities to assess the strength of events belonging to Class I and II. While formation rates (J) are usually calculated for 10 nm particles (J_{10}), sampling line issues causing high variability of the sub-16 nm concentrations in Cap Es Pinar (see Fig. 7) only allowed for calculations involving larger diameter particle concentrations (J_{16}). In order to ease the comparison between Ersa and Cap Es Pinar, a similar size range was applied for J calculation from the Ersa dataset. For comparison with the literature, one has to keep in mind that J_{16} are lower than J_{10}, due to coagulation effects during the growth of the particles from 10 nm to 16 nm.

Growth rates (GR) were calculated from the SMPS nucleation mode concentrations (16-20 nm) using the "maximum" method from Hirsikko et al.(2005). The time corresponding to the maximum concentration was first determined for each of the SMPS size channels in the range 16 – 20 nm by fitting a normal distribution to the concentration. The growth rate was then derived from a linear least square fit through these time values.

From this growth rate, we derived the total particle formation rate at 16 nm (J_{16}), similarly as in Dal Maso et al. (2005) using the following equation (Eq.1) :

$$J_{16} = \frac{dN_{16}}{dt} + CoagS_{16} \times N_{16} + \frac{GR_{16-20}}{(20-16)nm} \times N_{16} \quad (1)$$

$CoagS_{16}$ is the coagulation sink of 16 nm particles on larger particles, N_{16} is the total concentration of 16-20 nm particles and GR_{16-20} is the growth rate corresponding to the same diameter range.

4 Results and discussion

4.1 Yearly statistical analysis of NPF events characteristics at two ground-based stations

The goal of this first section is to provide an overview of the seasonal variability of NPF in the Mediterranean area, and some insights into the spatial homogeneity of the NPF occurrence over the basin.

4.1.1 NPF Events frequency and types

The yearly average NPF frequencies, calculated as the number of event days over the total number of measurement days, are very similar at Finokalia and Ersa, being 36% (109 events) and 35% (96 events), respectively (Table 1). A comparable value was reported by Pikridas et al. (2012) at Finokalia, with a yearly average frequency of ~ 33% calculated over a year from April 2008 to April 2009. At both stations, the NPF frequency shows a clear annual cycle with the highest frequencies observed during spring (52% in May for Finokalia and 56% in April for Ersa), and the lowest in autumn (Fig. 2). A similar seasonal variation was previously reported for Finokalia, with a slight time offset of the NPF frequency peak observed in February-March (Pikridas et al., 2012). More generally, higher NPF frequencies are frequently observed during spring (April-May-June) compared to the rest of the year at European stations (Manninen et al., 2010). As previously suggested by Manninen et al. (2010, and references therein) and further supported by Fig. S1, higher NPF frequencies in spring are most probably related to the onset of biogenic emissions which is favored by increasing temperatures, together with higher solar radiation enhancing the production of low volatile oxidized vapors.

The classification of the event days into the different categories (Fig. 3 and Table 1) shows that the occurrence of type I events in Finokalia follows the same seasonal variation as the total NPF frequency, being maximum during the spring season (up to 26% of all days). This indicates that spring is favorable to both formation of new particles and their growth to larger sizes. Type II events are annually the most frequent, representing between 13% and 31% of all measurement days with no clear seasonal variation. In contrast, undefined days are not frequently observed in Finokalia, around 9% on average. Very similar features are observed in Ersa: type I events show the highest frequency of occurrence during spring and summer (up to 32% of all days in August), while they represent less than 10% of the measurement days during winter. The frequency of occurrence of type II events is on average 19%, with no clear seasonal variation.

4.1.2 Growth rates and particle formation rates

Particle formation and growth rates were calculated for type I events in order to characterize the strength of the events observed at the two stations. The yearly median particle growth rates in the range 16 – 20 nm (GR_{16-20}) are 7.10 and 16.7 nm h^{-1} at Ersa and Finokalia, respectively (Table 2). The values obtained at Finokalia are in the upper range of the values reported by Manninen et al. (2010) at European sites for 7 – 20 nm diameter particles (1.8 – 20 nm h^{-1}, mean value 4.4 nm h^{-1}). Especially, the values calculated in this work are on average higher compared to those obtained at other European coastal sites such as Cabauw (2.1 - 19 nm h^{-1}, mean value 6.7 nm h^{-1}) and Mace Head (2.7 – 10 nm h^{-1}, mean year value 5.4 nm h^{-1}) (Manninen et al., 2010). Higher growth rates are expected in environments with high solar radiation and emissions, such as the Mediterranean basin. However, the median value reported here is also higher than the one reported for Finokalia from the years 2008-2009 in the size range 7 – 20 nm (5 nm h^{-1}) (Manninen et al., 2010). This result may be explained by the higher size range used here for the GR calculation (16-20nm instead of 7-20 nm), which leads to higher values because GR usually increases with particle size, but also higher uncertainty because of the narrow size range. Figure 4 displays the annual variation of the particle growth rates at Ersa and Finokalia. At Ersa, GR have the same

seasonal variation as the NPF frequency, with higher values in spring compared to the rest of the year. At Finokalia, the GR seasonality is not as clear as in Ersa. However, the seasonality in Finokalia is rather biased because there are only few class I events during summer.

The yearly median particle formation rates (J_{16}) are 0.16 $cm^{-3}s^{-1}$ in Ersa and 0.26 $cm^{-3}s^{-1}$ in Finokalia (Table 2). These values are slightly lower than the J_{10} values reported by Kulmala et al. (2004) from several coastal sites and ship campaigns conducted in the Baltic, Atlantic and Pacific areas (0.4 – 1.5 $cm^{-3}s^{-1}$). Besides different environmental conditions which might explain these differences, one has to keep in might that J_{16} values are expected to be lower than J_{10} because of the coagulation processes which cause particle loss during their growth. The values calculated in this work are, to our knowledge, the first reported for the formation of nucleation mode particles (10 – 20 nm) in the Mediterranean basin. As shown on Fig. 5, median J_{16} also follows a seasonal variation similar to the NPF frequency at both stations, with higher values in spring (March, with 0.56 $cm^{-3}s^{-1}$ for Finokalia, and April, with 0.66 $cm^{-3}s^{-1}$ for Ersa). This observation suggests that condensable vapors needed to grow the clusters up to 16 nm are most likely of the same origin as those initiating the NPF process. In contrast, lower J_{16} are observed in early winter and mid-summer at both stations.

It is worth noticing that in Ersa, even though NPF frequencies are lower in autumn compared to spring, particle formation rates are comparable. This last observation suggests that, despite being less frequent, favorable conditions for NPF can be found during autumn and lead to events with the same intensity as in spring, when radiation and biogenic emissions are on average higher compared to the rest of the year (Manninen et al., 2010). The seasonal variation of nucleation frequency, nucleation rates and growth rates is most likely related the availability of condensable gases. The amount of such precursors results from the balance between a combination of emissions and radiation, that favor their production, and their loss onto preexisting particles. In order to assess the influence of the preexisting aerosol population on NPF, we calculated the condensational sink (CS) according to Pirjola et al. (1999). The CS was first derived from SMPS measurements for the whole measurement period at both stations and was finally averaged over the two-hour period prior to the onset of NPF events. On non-event days, the CS was averaged over the two-hours time period prior to the time at which NPF is triggered on event days, i.e. ~ 11:00 (UTC) in Finokalia and ~ 12:00 (UTC) in Ersa. The annual variation of the median CS derived from these averaged values is reported for event and non-event days on Fig. 6.

The CS has a strong seasonal cycle with a clear maximum during summer at both stations. This observation may explain the lower NPF frequencies, formation rates and growth rates that are on average observed during this season, that otherwise shows high radiation (Fig. S1), and most probably high biogenic emissions. In addition, the CS is on average higher during non-event days at both stations. This confirms that the CS is likely a limiting factor for the occurrence of NPF at these stations. This was already pointed out by Kulmala et al. (2005), Hamed et al. (2010) and Manninen et al. (2010) for several boundary layer stations in Europe, including both industrialized locations and more pristine areas, such as boreal forest. One should however note that during spring months (especially March and April), median CS is similar on event and non-event days. This observation suggests that during this period, the strength of precursors emissions together with radiation might be driving the occurrence NPF to a major extent. Also, the CS is on average higher in Finokalia, especially during spring and summer with monthly CS twice as high compared to Ersa. It is worth noticing that large particles up to 848 nm are accounted for in the CS calculation in Finokalia, while the upper size limit is 495 nm in Ersa. However,

particles above 500 nm only have a weak impact on the Cs values due to their low concentration, and thus do not explain the differences which are seen between the sites. At Finokalia, north-northeastern winds dominate during summer, bringing high concentrations of anthropogenic aerosol that have aged when passing over the sea before reaching the station, thus leading to high CS values. The fact that NPF frequencies, nucleation rates and growth rates are comparable at the two stations indicates that the sources of condensable gases are likely to be significantly higher in Finokalia compared to Ersa in order to compensate for the large condensational sink measured at the Greek station.

Based on the previous observations, Finokalia and Ersa show similar seasonality in the average nucleation frequency, growth rates and nucleation rates although the two stations are more than 1000 km away from each other. It is worth mentioning that during the period of interest, 109 event days were observed at Finokalia and 96 at Ersa, among which 31 (with 8 events of class I) occurred at both stations at the same time. These results could indicate that the spatial extent of NPF events over the Mediterranean basin is at the synoptic scale, and in the order of the distance between the two stations, i.e. more than 1000 km. Such a conclusion was already drawn from observations of NPF events at three stations located in northern Europe (Vana et al. 2004). However, we will downscale the comparison of occurrence and characteristics of events at the daily resolution (rather than monthly), in order to further investigate this hypothesis.

4.2 Intensive campaign during summer 2013

4.2.1 Ground-based measurements - overview

In this section, we focus on the Special Observation Period (SOP) that took place from June 3rd to August 12th in the frame of the CHARMEX project. During this period, number size distribution measurements were additionally conducted at the Mallorca station (Cap Es Pinar).

Figure 7 shows the SMPS particle size distributions recorded at the three ground-based stations during the SOP. From this synoptic overview, we clearly observe similar trends in the evolution of the particle size distributions in Ersa and Cap Es Pinar, with three distinct NPF periods during which NPF events occurred daily over several days (First period from July 4th to July 9th, second period from July 28th to August 3rd and third period from August 9th to August 12th) (see Table S1). This observation would confirm the spatial extent of NPF events at a large scale. However, these periods of intense NPF activity were not observed in Finokalia, where both the occurrence and strength of NPF events seem to be more homogeneous over the SOP. These contrasting observations might be explained by an environmental contrast between the eastern and western part of the Mediterranean basin.

As reported in Table S1, during this 41-days period, NPF was observed to occur at one station (at least) on 23 days. Among these 23 event days, 8 events were observed on the same day on two stations at least. This frequency of simultaneous NPF events occurrence is very similar to the one observed at Korean coastal sites (5 out of 21 observation days, Kim et al. 2016). NPF was detected at all sites on August 9th, and three events were reported on the same day for each of the station pairs Ersa – Finokalia and Ersa – Mallorca, and one event for the pair Finokalia - Mallorca. In order to further investigate the link that might exist between the events observed at the three stations, we first chose to focus our analysis on three days that belong to the three different NPF periods identified: July 5th, July 29th and August 9th are presented as case studies. Type one events were observed in Ersa

and Cap Es Pinar on those specific days, thus allowing for particle formation and growth rates calculations, and further direct comparison of event intensity at these two sites.

4.2.2 Ground-based measurements: Case studies

We calculated the total formation rate of 20 nm particles (J_{20}) using particle growth rates in the size range 15-25 nm (GR_{15-25}, Table 3) for the three cases: July 5th, July 29th and August 9th. We first shortly describe the NPF events observed on the 5th and 29th of July (fully described in the supplementary) and then illustrate in more details the events observed on the 9th of august that have the most similarities between sites.

On July 5th, although NPF occurs both at Ersa and Cap Es Pinar, the time evolution of particle concentrations are very different from one site to the other. Particles of the smallest size range are detected in the morning at Ersa, but ony later in the afternoon at Cap es Pinar, and at larger sizes and lower concentrations (Fig. S2). The 24-hour air mass back trajectory analysis (HYSPLIT transport and dispersion model, Draxler et al. 2003) shows that air masses arriving at both stations are of northerly origin (Fig. S3). Hence it is unlikely that particles formed during the NPF event detected at Ersa in the morning have been transported west and detected later in the afternoon at Cap Es Pinar.

In order to further evaluate the spatial extent of nucleation, we estimated for each site the distance between the station the place where nucleation was initially triggered upstream the station. The method we used is based on the time evolution of the aerosol size distribution and was previously described by Rose et al. (2015b). We assumed that 20 nm particles detected at the station were originally formed by NPF and that nucleated clusters had a diameter of 1 nm. The time required for a cluster to grow between 1 and 20 nm was first calculated using GR_{15-25}. Then, knowing the time corresponding to the maximum concentration of 20 nm particles at the station, we were able to calculate the time at which nucleation occurred. Finally, using air mass back trajectories we determined the location where nucleation had been triggered upstream the station. It is worth noticing that since particle growth rates were reported to increase with particle size (Yli-Juuti et al, 2011), GR_{15-25} provide an underestimation of the particle growth time between 1 and 20 nm, and therefore a lower limit of the distance between the place where nucleation is initially triggered and the station.

On July 5th, previous calculations lead to distances of at least 9 km (Ersa) and 40 km (Cap Es Pinar) upstream the stations, which thus cannot allow further conclusions on the simultaneity of a large NPF covering the spatial area of both stations. The event of July 29th is detected from the lowest sizes of the SMPS at both stations with the same intensity (similar N_{15-20} and J_{20}), and show similar features (Fig. S4), but is detected one hour earlier at Cap Es Pinar than at Ersa. Air masses were from the northern sector at Cap Es Pinar, and then turned west towards Ersa (Fig. S6).

In Finokalia, both for July 5th and July 29th, significant N_{15-20} concentration are also detected during the nucleation hours, but in the form of a succession of peaks that do not show the usual feature of a clear NPF event (with a continuous growth).

On August 9th, newly formed particles are detected in air masses originating from the near southern area in Ersa and from northwestern sector in Cap Es Pinar (see Fig.9). The concentration of particles mesured in the first SMPS size channels in Ersa (11-15 nm) does not present very marked variations, while N_{15-20} displays more

significant changes in the course of the day. These observations might suggest that unlike previous events, NPF could not be initiated at the station itself, but rather in a neighbouring area (Fig. 8). Similar features are observed at Cap Es Pinar, with significant variations of the particle concentration in the size range 15-20 nm, as on July 29th. The temporal evolutions of N_{15-20} and N_{20-25} have similar structures at both stations between 10:00 and 16:00 UTC, suggesting that NPF could occur simultaneously at both sites. Additional peaks of N_{15-20} and N_{20-25} are detected earlier in the morning at Cap Es Pinar (7:20 and 9:00 UTC), while they are not detected in Ersa. Beside the simultaneity of the process, NPF events detected at the two sites also display very similar characteristics, both regarding particle growth (4.3 and 3.8 nm h^{-1}, for Ersa and Cap Es Pinar, respectively) and formation rates (4.83 and 4.17 cm^{-3} s^{-1}, for Ersa and Cap Es Pinar, respectively). Instrumental failure did not allow similar analysis at Finokalia.

As shown on Fig. 9 for Cap Es Pinar, the place where nucleation initially occurred is at least 49 km upstream the station. Since all air mass back trajectories computed during the time period of interest are very local (at least during the 24 hours before their arrival at the site), we may hypothesis that NPF is occuring over the whole area close to Mallorca where air mass backtrajectories overlap. Concerning Ersa, the nucleation of 20 nm particles latter observed at the site is at least initiated 45 km upstream the station.

The three case studies showed that NPF events could be detected, with some time offset, on two remote stations separated by several hundred kilometers in the Mediterranean area. In particular for the case of August 9th, the fact that these events can be detected in air masses from different origins suggest that the NPF is, for both sites, initiated above the sea, either in the marine boundary layer or higher in the free troposphere. In any case, the NPF process is likely not subject to the availablility of precursors that would be specific to the air mass type reaching the sites. It could rather depend on synoptic meteorological conditions at the European scale, including low condensational sinks following precipitations periods. Indeed, the analysis of the meteorological conditons along backtrajectories shows that precipitation did occur prior to their arrival at both stations on July 29th (during the passage of low pressure systems), but not on the two other case studies. The minimum areas that we determined for nucleation onset at both sites did not overlap. However, the estimates we obtained are some lower limits of the actual values, and there are no elements which could justify that the NPF was interrupted between both sites. Airborne measurements will be used in the next section to further investigate this aspect. In addition, these flights will allow an analysis regarding the origin of the clusters and their precursors, from the marine boundary layer or from the upper levels of the atmosphere, as previously shown by Rose et al. (2015a).

4.2.3 Airborne measurements

Among the 11 flights performed during the SOP period, particles in the lowest size range (N_{3-10}) were not observed during 7 of the flights, in agreement with no NPF events detected at the Ersa and Cap Es Pinar stations. Two flights detected elevated concentrations of N_{3-10} and N_{10-20} in agreement with NPF events at Ersa.

The first event to be investigated was observed on July 30th. Regarding aircraft measurements, the analysis was focused on the flight legs performed at constant altitude and during which N_{3-10} concentrations were above the threshold value (Fig. 10a). The first part of the flight was performed at low altitude (~ 215 m a.s.l.) from the french coast towards Ersa and at higher altitudes (~ 3400 m a.s.l.) during the second part of the flight from Ersa towards the coast. Based on Fig. 10, small particles (N_{3-10}) were detected at both altitudes and over a large area

included in a 219 × 131 km rectangle. On the low altitude flight section, $N_{3\text{-}10}$ is decreasing from the northeastern part of the flight track to the southwestern one. This would indicate a source of nanoparticles originating from the continent and progressively diluted in the marine boundary layer. However, despite a high variability, $N_{3\text{-}10}$ are on average higher at high altitude, with average concentrations of 3805±1555 cm^{-3} compared to 2040±2174 cm^{-3} at lower altitude. This last observation supports the results of Rose et al. (2015a) who reported that nucleation could be enhanced at high altitude above the Mediterranean Sea and connected to different sources at low altitude.

In order to explore the link that may exist between the events detected simultaneously from the aircraft and from the ground, we first investigated the origin of the air masses. Figure 10b shows the 72 hour back trajectories of the air masses sampled by the ATR-42 every 10 min along the flight path as well as the 72 hour back trajectories of the air masses that reached Ersa in the meanwhile at 13:00, 14:00 and 15:00 UTC. During the first part of the flight performed at low altitude, the aircraft flew in southern air masses which all passed over the continent before sampling and became more local as the aircraft approached Ersa. In contrast, the air masses sampled at high altitude were from western origin, so that they also passed over the continent, but did not display any local features.

In addition, Fig. 11 shows the evolution of the particle size distributions measured onboard the ATR-42 and at Ersa. The spectra are color coded according to the position of the aircraft indicated in the insert included in the middle panel of Fig. 11. At Ersa, the shape of the particle size distribution remains similar during the whole measurement period, with a nucleation mode around 20 – 25 nm, an Aitken mode around 50 – 60 nm which clearly dominates the spectra and two accumulation modes, respectively around 110 and 220 nm. These modes were identified when fitting the SMPS size distributions with four Gaussian modes using the methodology described in Rose et al. (2015a). In contrast, the size distributions provided by the SMPS onboard the ATR-42 show significant variations. Lower concentrations are on average observed at higher altitude for the whole diameter range but with more significant changes of the nucleation and Aitken modes. The shape of the size distribution is also impacted by the location of the plane, especially at low altitude. In fact, the total particle concentration decreases as the aircraft moves further off the southern coast of France, with, again, a more visible impact on nucleation and Aitken modes.

These last observations, together with the air mass back trajectory analysis shown on Fig. 10.b, suggest that for this first event, new particles were initially formed at low altitude over the continent and further transported above the sea to be finally detected over a large area, and more especially in Ersa. Decreasing particle concentrations observed while moving further off the continent make less probable the hypothesis of new small particles formation from an additional marine source, but rather depict the effect of dispersion process that may have taken place during particle transport.

The second event included in this analysis was observed on August 1st. Compared to the previous case study, the flight was performed over a larger area (172 × 247 km rectangle) located further away west from Ersa and at a relatively low constant altitude (~ 500 m a.s.l.). $N_{3\text{-}10}$ concentrations above the threshold value were detected along the flight path (Fig. 12) and compared well, on average, with the concentrations obtained at low altitude during the flight performed on July 30th (2483±2767 cm^{-3}). However, $N_{3\text{-}10}$ concentrations occurred as bursts, with no clear spatial gradient as previously reported for flight performed on July 30th. The analysis of air mass

back trajectories is shown on Fig 12.b. north-eastern air masses were sampled at the beginning and at the end of the flight, with northern air masses in between. Air masses from the north were also detected at Ersa and it is worth noticing that, at least during the first part of the flight, the air masses that reached the aircraft had all passed over Ersa region.

The evolution of the particle size distributions together with the location of the aircraft is shown in Fig. 13. Unlike during the flight performed on July 30th, the shape of the distributions measured onboard the ATR-42 remains similar during the whole measurement period despite the changing origin of air masses. In contrast, the shape of the particle size distributions measured at Ersa shows a significant variability. Especially, the nucleation mode displays increasing diameters from 20 to 30 nm and highly variable concentrations. Also, total concentrations from Ersa are significantly higher compared to those measured onboard the ATR-42.

In order to further investigate the origin of the nucleation mode particles and the connection that may exist between ground based and airborne measurements, we compared the diameters of the corresponding nucleation modes. For that purpose, Fig. 14 shows the ratio of the nucleation mode diameter obtained onboard the ATR-42 over that from Ersa as a function of the distance between the aircraft and the station. This ratio is in the range 0.6 – 1.2, with on average decreasing values while increasing the distance between the two measurement points. Nucleation mode diameter getting smaller along the air mass back trajectory above the sea could be the result of intense inputs of nucleated particles initially below the SMPS size detection limit and feeding the nucleation mode as they grow, as confirmed by the occurrence of $N_{3\text{-}10}$ nm particles detected in the ATR-42. In this particular case, particles detected in the nucleation mode observed onboard the ATR-42 would be the result of an event occurring above the sea from marine precursors, which superimposes with a preexisting particle mode.

5 Conclusion

We investigated the occurrence of NPF in the Mediterranean area using particle size distributions measured at three ground-based stations (Ersa, Cap Es Pinar and Finokalia) as well as airborne measurements performed in 2013 in the frame of the CHARMEX-ADRIMED and CHARMEX-SafMed projects.

The analysis of long-term datasets from Ersa and Finokalia first revealed similar features, although the two stations are more than 1000 km away from each other. Especially, almost equal annual NPF frequencies were reported (36% and 35%, for Finokalia and Ersa, respectively) and similar seasonal variations of both the NPF frequency and characteristics, i.e. particle formation and growth rates, were observed. The NPF process was on average favored during spring, both in terms of occurrence and intensity, most probably because of increased amounts of precursors from biogenic origin and higher solar radiation, thus allowing for more efficient photochemistry processes.

This investigation, initially performed at a monthly resolution was downscaled in a second step at the daily resolution over a two months period, in order to further assess the simultaneity of NPF over a large part of the Mediterranean basin. Three simultaneous nucleation periods of several days appeared clearly for Ersa and Cap Es Pinar, and less clearly at Finokalia. NPF formation was observed to occur simultaneously at least at two of the three stations on 8 days over the 41 days of observation, which confirms the frequent occurrence of regional

scale NPF events in the Mediterranean area. Three case study events were selected within these three distinct NPF periods for a more detailed analysis. These three case studies showed that NPF events could be detected, with some time offset, on two remote stations separated by several hundred kilometers in the Mediterranean basin, without the stations being directly linked to eachother within a single air mass trajectory. While featuring local characteristics, the occurrence of NPF events was likely not dependant on the availablility of precursors that would be specific to the air mass type reaching the sites, but rather on synoptic meteorological conditions at the European scale. Kompula et al. (2006) also concluded from observation from two different sites 250 km appart, that the occurrence of of NPF in a certain air mass type depended not only on the local conditions promoting the process (such as photochemistry), but also on some properties carried by the air mass itself. Likewise, Hussein et al. (2009) showed from a multisites observations dataset in Scandinavia that although large spatial scale NPF events were observed simultaneously bewteen several stations, their characteristics usually differ in term of temporal evolution, due to different local meteorological conditions, and maybe variable local emissions.

The case studies also showed that despite the fact that nucleation monthly frequencies, monthly nucleation rates and growth rates had similar seasonnal variations in Ersa and Finokalia, different behaviors were observed on a daily basis between the western and eastern mediterranean bassins. Again, the combination of favourable synoptic conditions and seasonnal variations in general emission schemes may favour a seasonnal behavior of the NPF frequency and characteristics, but local conditions are modulating the general behavior of regional NPF.

Airborne measurements were finally used to further investigate the horizontal and vertical extent of NPF, and to determine the origin of the clusters and their precursors. Two case studies were again selected within the NPF periods identified previously from ground-based observations, during which newly formed clusters were observed onboard the ATR-42 and from Ersa on the same day. Airborne measurements confirmed the regional spatial extend of NPF events, and further showed regional NPF events can have different sources. The selected events depicted contrasting situations where particles were initially probably formed above the continent for one of them, both in the boundary layer and in the free troposphere, and probably formed above the sea for the other.

This work, together with the previous study by Rose et al. (2015a), demonstrates the occurrence of NPF in the Mediterranean basin, thus highlighting the possibility for the process to be triggered above open seas. Those results are of great interest to improve the parameterizations of nucleation in models, which actually only consider a limited number of precursors, commonly including sulfuric acid and ammonia but excluding those more specifically emitted in the marine atmosphere. Model predictions would also benefit from the analysis of the vertical extent of the NPF process provided in these studies. Besides the identification of preferential altitudes for the occurrence of the process, these results aid understanding the transport of the newly formed clusters and their precursors between the boundary layer and the free troposphere. Future studies should focus on understanding the chemical precursors that contribute to these new particle formation processes.

Ackowledgements

This study was performed with the financial support of the French National Research Agency (ANR) project ADRIMED (contract ANR-11-BS56-0006) the ANR project SAf-Med “” (Grant Number: SIMI-5-6 022 04) and is part of the ChArMEx project supported by ADEME, CEA, CNRS-INSU and Météo-France through the multidisciplinary programme MISTRALS (Mediterranean Integrated Studies aT Regional And Local

Scales). The Financial support for the ACTRIS Research Infrastructure Project by the European Union's Horizon 2020 research and innovation program under grant agreement no. 654169 and previously Under grant agreement no. 262254 in the 7th Framework Programme (FP7/2007–2013) is gratefully acknowledged.

References

Birmili, W., Berresheim, H., Plass-Dülmer, C., Elste, T., Gilge, S., Wiedensohler, A. and Uhrner, U.: The Hohenpeissenberg aerosol formation experiment (HAFEX): a long-term study including size-resolved aerosol, H 2 SO 4, OH, and monoterpenes measurements, Atmospheric Chem. Phys., 3(2), 361–376, 2003.

Crippa, P. and Pryor, S. C.: Spatial and temporal scales of new particle formation events in eastern North America, Atmos. Environ., 75, 257–264, doi:10.1016/j.atmosenv.2013.04.051, 2013.

Crumeyrolle, S., Manninen, H. E., Sellegri, K., Roberts, G., Gomes, L., Kulmala, M., Weigel, R., Laj, P. and Schwarzenboeck, A.: New particle formation events measured on board the ATR-42 aircraft during the EUCAARI campaign, Atmospheric Chem. Phys., 10(14), 6721–6735, doi:10.5194/acp-10-6721-2010, 2010.

Cusack, M., Pérez, N., Pey, J., Alastuey, A. and Querol, X.: Source apportionment of fine PM and sub-micron particle number concentrations at a regional background site in the western Mediterranean: a 2.5 year study, Atmospheric Chem. Phys., 13(10), 5173–5187, doi:10.5194/acp-13-5173-2013, 2013.

Dal Maso, M., Kulmala, M., Riipinen, I., Wagner, R., Hussein, T., Aalto, P. P. and Lehtinen, K. E. J.: Formation and growth of fresh atmospheric aerosols : eight years of aerosol size distribution data from SMEAR II, Hyytiälä, Finland, Boreal Environ. Res., 10(5), 323–336, 2005.

Dall'Osto, M., Querol, X., Alastuey, A., O'Dowd, C., Harrison, R. M., Wenger, J. and Gómez-Moreno, F. J.: On the spatial distribution and evolution of ultrafine particles in Barcelona, Atmospheric Chem. Phys., 13(2), 741–759, doi:10.5194/acp-13-741-2013, 2013.

Draxler, R. R. and Rolph, G. D.: HYSPLIT (Hybrid Single-Particle Langrangian Integrated Trajectory) Model access via NOAA ARL READY website (http://www.arl.noaa.gov/ready/hysplit4.html), 2003.

Hamed, A., Birmili, W., Joutsensaari, J., Mikkonen, S., Asmi, A., Wehner, B., Spindler, G., Jaatinen, A., Wiedensohler, A., Korhonen, H. and others: Changes in the production rate of secondary aerosol particles in Central Europe in view of decreasing SO 2 emissions between 1996 and 2006, Atmospheric Chem. Phys., 10(3), 1071–1091, 2010.

Hirsikko, A., Laakso, L., Hörrak, U., Aalto, P. P., Kerminen, V.-M. and Kulmala, M.: Annual and size dependent variation of growth rates and ion concentrations in boreal forest, Boreal Environ. Res., 10(5), 357–369, 2005.

Hirsikko, A., Bergman, T., Laakso, L., Maso, M. D., Riipinen, I., Horrak, U. and Kulmala, M.: Identification and classification of the formation of intermediate ions measured in boreal forest, Atmospheric Chem. Phys., 7(1), 201–210, 2007.

Hussein, T., Junninen, H., Tunved, P., Kristensson, A., Dal Maso, M., Riipinen, I., Aalto, P. P., Hansson, H.-C., Swietlicki, E. and Kulmala, M.: Time span and spatial scale of regional new particle formation events over Finland and Southern Sweden, Atmos Chem Phys, 9(14), 4699–4716, 2009.

Jeong, C.-H., Hopke, P. K., Chalupa, D. and Utell, M.: Characteristics of Nucleation and Growth Events of Ultrafine Particles Measured in Rochester, NY, Environ. Sci. Technol., 38(7), 1933–1940, doi:10.1021/es034811p, 2004.

Kalivitis, N., Birmili, W., Stock, M., Wehner, B., Massling, A., Wiedensohler, A., Gerasopoulos, E. and Mihalopoulos, N.: Particle size distributions in the Eastern Mediterranean troposphere, Atmospheric Chem. Phys., 8(22), 6729–6738, 2008.

Kalivitis, N., Stavroulas, I., Bougiatioti, A., Kouvarakis, G., Gagné, S., Manninen, H. E., Kulmala, M. and Mihalopoulos, N.: Night-time enhanced atmospheric ion concentrations in the marine boundary layer, Atmospheric Chem. Phys., 12(8), 3627–3638, doi:10.5194/acp-12-3627-2012, 2012.

Kalivitis, N., Kerminen, V.-M., Kouvarakis, G., Stavroulas, I., Bougiatioti, A., Nenes, A., Manninen, H. E., Petäjä, T., Kulmala, M. and Mihalopoulos, N.: Atmospheric new particle formation as a source of CCN in the eastern Mediterranean marine boundary layer, Atmos Chem Phys, 15(16), 9203–9215, doi:10.5194/acp-15-9203-2015, 2015.

Kim, Y., Kim, S.-W., Yoon, S.-C., Park, J.-S., Lim, J.-H., Hong, J., Lim, H.-C., Ryu, J., Lee, C.-K. and Heo, B.-H.: Characteristics of formation and growth of atmospheric nanoparticles observed at four regional background sites in Korea, Atmos. Res., 168, 80-91, doi.org/10.1016/j.atmosres.2015.08.020, 2016.

Komppula, M., Sihto, S.-L., Korhonen, H., Lihavainen, H., Kerminen, V.-M., Kulmala, M., and Viisanen, Y.: New particle formation in air mass transported between two measurement sites in Northern Finland, Atmos. Chem. Phys., 6, 2811-2824, doi:10.5194/acp-6-2811-2006, 2006.

Koren, I., Dagan, G., Altaratz, O. and others: From aerosol-limited to invigoration of warm convective clouds, Science, 344(6188), 1143–1146, 2014.

Kouvarakis, G., Tsigaridis, K., Kanakidou, M. and Mihalopoulos, N.: Temporal variations of surface regional background ozone over Crete Island in the southeast Mediterranean, J. Geophys. Res. Atmospheres 1984–2012, 105(D4), 4399–4407, 2000.

Kristensson, A., Johansson, M., Swietlicki, E., Kivekäs, N., Hussein, T., Nieminen, T., Kulmala, M. and Dal Maso, M.: NanoMap: Geographical mapping of atmospheric new particle formation through analysis of 1 particle number size distribution data 2 3 Short version of title:"NanoMap: Mapping of new particle formation events" 4 5, [online] Available from: http://www.cast.lu.se/Kristensson%20-%20NanoMap%20paper%20v4.pdf (Accessed 14 March 2016), 2014.

Kulmala, M., Vehkamäki, H., Petäjä, T., Dal Maso, M., Lauri, A., Kerminen, V.-M., Birmili, W. and McMurry, P. H.: Formation and growth rates of ultrafine atmospheric particles: a review of observations, J. Aerosol Sci., 35(2), 143–176, 2004.

Kulmala, M., Petäjä, T., Mönkkönen, P., Koponen, I. K., Dal Maso, M., Aalto, P. P., Lehtinen, K. E. J. and Kerminen, V.-M.: On the growth of nucleation mode particles: source rates of condensable vapor in polluted and clean environments, Atmos Chem Phys, 5, 409–416, 2005.

Makkonen, R., Asmi, A., Kerminen, V.-M., Boy, M., Arneth, A., Hari, P. and Kulmala, M.: Air pollution control and decreasing new particle formation lead to strong climate warming, Atmospheric Chem. Phys., 12(3), 1515–1524, doi:10.5194/acp-12-1515-2012, 2012.

Mallet, M., Dulac, F., Formenti, P., Nabat, P., Sciare, J., Roberts, G., Pelon, J., Ancellet, G., Tanré, D., Parol, F., Denjean, C., Brogniez, G., di Sarra, A., Alados-Arboledas, L., Arndt, J., Auriol, F., Blarel, L., Bourrianne, T., Chazette, P., Chevaillier, S., Claeys, M., D'Anna, B., Derimian, Y., Desboeufs, K., Di Iorio, T., Doussin, J.-F., Durand, P., Féron, A., Freney, E., Gaimoz, C., Goloub, P., Gómez-Amo, J. L., Granados-Muñoz, M. J., Grand, N., Hamonou, E., Jankowiak, I., Jeannot, M., Léon, J.-F., Maillé, M., Mailler, S., Meloni, D., Menut, L., Momboisse, G., Nicolas, J., Podvin, T., Pont, V., Rea, G., Renard, J.-B., Roblou, L., Schepanski, K., Schwarzenboeck, A., Sellegri, K., Sicard, M., Solmon, F., Somot, S., Torres, B., Totems, J., Triquet, S., Verdier, N., Verwaerde, C., Waquet, F., Wenger, J. and Zapf, P.: Overview of the Chemistry-Aerosol Mediterranean Experiment/Aerosol Direct Radiative Forcing on the Mediterranean Climate (ChArMEx/ADRIMED) summer 2013 campaign, Atmospheric Chem. Phys., 16(2), 455–504, doi:10.5194/acp-16-455-2016, 2016.

Manninen, H. E., Nieminen, T., Asmi, E., Gagné, S., Häkkinen, S., Lehtipalo, K., Aalto, P., Vana, M., Mirme, A., Mirme, S., Hõrrak, U., Plass-Dülmer, C., Stange, G., Kiss, G., Hoffer, A., Törő, N., Moerman, M., Henzing, B., de Leeuw, G., Brinkenberg, M., Kouvarakis, G. N., Bougiatioti, A., Mihalopoulos, N., O'Dowd, C., Ceburnis, D., Arneth, A., Svenningsson, B., Swietlicki, E., Tarozzi, L., Decesari, S., Facchini, M. C., Birmili, W., Sonntag, A., Wiedensohler, A., Boulon, J., Sellegri, K., Laj, P., Gysel, M., Bukowiecki, N., Weingartner, E., Wehrle, G., Laaksonen, A., Hamed, A., Joutsensaari, J., Petäjä, T., Kerminen, V.-M. and Kulmala, M.: EUCAARI ion spectrometer measurements at 12 European sites – analysis of new particle formation events, Atmos Chem Phys, 10(16), 7907–7927, doi:10.5194/acp-10-7907-2010, 2010.

583 Merikanto, J., Spracklen, D. V., Mann, G. W., Pickering, S. J. and Carslaw, K. S.: Impact of nucleation on global
584 CCN, Atmospheric Chem. Phys., 9(21), 8601–8616, 2009.

585 Mihalopoulos, N., Stephanou, E., Kanakidou, M., Pilitsidis, S. and Bousquet, P.: Tropospheric aerosol ionic
586 composition in the Eastern Mediterranean region, Tellus, 49B, 314–326, 1997.

587 Nabat, P., Somot, S., Mallet, M., Chiapello, I., Morcrette, J. J., Solmon, F., Szopa, S., Dulac, F., Collins, W.,
588 Ghan, S., Horowitz, L. W., Lamarque, J. F., Lee, Y. H., Naik, V., Nagashima, T., Shindell, D. and Skeie, R.: A
589 4-D climatology (1979–2009) of the monthly tropospheric aerosol optical depth distribution over the
590 Mediterranean region from a comparative evaluation and blending of remote sensing and model products,
591 Atmospheric Meas. Tech., 6(5), 1287–1314, doi:10.5194/amt-6-1287-2013, 2013.

592 Pey, J., Rodríguez, S., Querol, X., Alastuey, A., Moreno, T., Putaud, J. P. and Van Dingenen, R.: Variations of
593 urban aerosols in the western Mediterranean, Atmos. Environ., 42(40), 9052–9062,
594 doi:10.1016/j.atmosenv.2008.09.049, 2008.

595 Pikridas, M., Bougiatioti, A., Hildebrandt, L., Engelhart, G. J., Kostenidou, E., Mohr, C., Prévôt, A. S. H.,
596 Kouvarakis, G., Zarmpas, P., Burkhart, J. F., Lee, B.-H., Psichoudaki, M., Mihalopoulos, N., Pilinis, C., Stohl,
597 A., Baltensperger, U., Kulmala, M. and Pandis, S. N.: The Finokalia Aerosol Measurement Experiment – 2008
598 (FAME-08): an overview, Atmospheric Chem. Phys., 10(14), 6793–6806, doi:10.5194/acp-10-6793-2010, 2010.

599 Pikridas, M., Riipinen, I., Hildebrandt, L., Kostenidou, E., Manninen, H., Mihalopoulos, N., Kalivitis, N.,
600 Burkhart, J. F., Stohl, A., Kulmala, M. and Pandis, S. N.: New particle formation at a remote site in the eastern
601 Mediterranean, J. Geophys. Res. Atmospheres, 117(D12), D12205, doi:10.1029/2012JD017570, 2012.

602 Pirjola, L., Kulmala, M., Wilck, M., Bischoff, A., Stratmann, F. and Otto, E.: Formation of sulphuric acid
603 aerosols and cloud condensation nuclei: an expression for significant nucleation and model comparison, J.
604 Aerosol Sci., 30(8), 1079–1094, doi:10.1016/S0021-8502(98)00776-9, 1999.

605 Rose, C., Sellegri, K., Freney, E., Dupuy, R., Colomb, A., Pichon, J.-M., Ribeiro, M., Bourianne, T., Burnet, F.
606 and Schwarzenboeck, A.: Airborne measurements of new particle formation in the free troposphere above the
607 Mediterranean Sea during the HYMEX campaign, Atmospheric Chem. Phys., 15(17), 10203–10218,
608 doi:10.5194/acp-15-10203-2015, 2015a.

609 Rose, C., Sellegri, K,, Velarde, F., Moreno, I., Ramonet, M., Weinhold,, K., Krejci, R., Andrade, M.,
610 Wiedensohler, A., and Laj, P.: Multiple daytime nucleation events at the high altitude station of Chacaltaya
611 (5240 m a.s.l.), Bolivia, Atmos. Environ., 102, 18–29, doi:10.1016/j.atmosenv.2014.11.015, 2015b.

612 Rosenfeld, D., Sherwood, S., Wood, R. and Donner, L.: Climate Effects of Aerosol-Cloud Interactions, Science,
613 343(6169), 379–380, doi:10.1126/science.1247490, 2014.

614 Sihto, S.-L., Kulmala, M., Kerminen, V.-M., Maso, M. D., Petäjä, T., Riipinen, I., Korhonen, H., Arnold, F.,
615 Janson, R., Boy, M. and others: Atmospheric sulphuric acid and aerosol formation: implications from
616 atmospheric measurements for nucleation and early growth mechanisms, Atmospheric Chem. Phys., 6(12),
617 4079–4091, 2006.

618 Sciare, J., K. Oikonomou, O. Favez, Z. Markaki, E. Liakakou, H. Cachier, and N.Mihalopoulos, Long-term
619 measurements of carbonaceous aerosols in the Eastern Mediterranean: Evidence of long-range transport of
620 biomass burning, Atmos. Chem. Phys., 8, 5551-5563, 2008

621 Spracklen, D. V., Carslaw, K. S., Kulmala, M., Kerminen, V.-M., Sihto, S.-L., Riipinen, I., Merikanto, J., Mann,
622 G. W., Chipperfield, M. P., Wiedensohler, A., Birmili, W. and Lihavainen, H.: Contribution of particle formation
623 to global cloud condensation nuclei concentrations, Geophys. Res. Lett., 35(6), doi:10.1029/2007GL033038,
624 2008.

625 Tao, W.-K., Chen, J.-P., Li, Z., Wang, C. and Zhang, C.: Impact of aerosols on convective clouds and
626 precipitation, Rev. Geophys., 50(2), doi:10.1029/2011RG000369, 2012.

627 Vana, M., Kulmala, M., Dal Maso, M., Hõrrak, U., and Tammet E.: Comparative study of nucleation mode
628 aerosol particles and intermediate air ions formation events at three sites, J. Geophys. Res., 109, D17201,
629 doi:10.1029/2003JD004413, 2004.

630 Weigel, R., Hermann, M., Curtius, J., Voigt, C., Walter, S., Böttger, T., Lepukhov, B., Belyaev, G. and
631 Borrmann, S.: Experimental characterization of the COndensation PArticle counting System for high altitude
632 aircraft-borne application, Atmospheric Meas. Tech., 2, 243–258, 2009.

633 Wiedensohler, A., Birmili, W., Nowak, A., Sonntag, A., Weinhold, K., Merkel, M., Wehner, B., Tuch, T.,
634 Pfeifer, S., Fiebig, M., Fjäraa, A. M., Asmi, E., Sellegri, K., Depuy, R., Venzac, H., Villani, P., Laj, P., Aalto, P.,
635 Ogren, J. A., Swietlicki, E., Williams, P., Roldin, P., Quincey, P., Hüglin, C., Fierz-Schmidhauser, R., Gysel, M.,
636 Weingartner, E., Riccobono, F., Santos, S., Grüning, C., Faloon, K., Beddows, D., Harrison, R., Monahan, C.,
637 Jennings, S. G., O'Dowd, C. D., Marinoni, A., Horn, H.-G., Keck, L., Jiang, J., Scheckman, J., McMurry, P. H.,
638 Deng, Z., Zhao, C. S., Moerman, M., Henzing, B., de Leeuw, G., Löschau, G. and Bastian, S.: Mobility particle
639 size spectrometers: harmonization of technical standards and data structure to facilitate high quality long-term
640 observations of atmospheric particle number size distributions, Atmospheric Meas. Tech., 5(3), 657–685,
641 doi:10.5194/amt-5-657-2012, 2012.

642 Yli-Juuti, T., Riipinen, I., Aalto, P. P., Nieminen, T., Maenhaut, W., Janssens, I. A., Claeys, M., Salma, I.,
643 Ocskay, R. and Hoffer, A.: Characteristics of new particle formation events and cluster ions at K-puszta,
644 Hungary, Boreal Environ. Res., 14(4), 683–698, 2009.

645 Yli-Juuti, T., Nieminen, T., Hirsikko, A., Aalto, P. P., Asmi, E., Hõrrak, U., Manninen, H. E., Patokoski, J., Dal
646 Maso, M., Petäjä, T., Rinne, J., Kulmala, M. and Riipinen, I.: Growth rates of nucleation mode particles in
647 Hyytiälä during 2003-2009: variation with particle size, season, data analysis method and ambient conditions,
648 Atmospheric Chem. Phys., 11(24), 12865–12886, doi:10.5194/acp-11-12865-2011, 2011.

649 Young, L.-H., Benson, D. R., Montanaro, W. M., Lee, S.-H., Pan, L. L., Rogers, D. C., Jensen, J., Stith, J. L.,
650 Davis, C. A., Campos, T. L., Bowman, K. P., Cooper, W. A. and Lait, L. R.: Enhanced new particle formation
651 observed in the northern midlatitude tropopause region, J. Geophys. Res., 112(D10),
652 doi:10.1029/2006JD008109, 2007.

653

Tables

Table 1 Classification of measurement days in Ersa and Finokalia (after filtering bad data).

	Number of measurements days	Event days		Undefined days	Non-event days
		Type I	Type II		
Ersa	276	43	53	23	157
Finokalia	301	38	71	27	165

Table 2 Annual median formation rates, growth rates and annual Cs in Ersa and Finokalia. Percentiles are also reported as additional information.

	J_{16} (cm^{-3} s^{-1})			GR_{16-20} (nm h^{-1})			CS (s^{-1})		
	25^{th} perc.	Med.	75^{th} perc.	25^{th} perc.	Med.	75^{th} perc.	25^{th} perc.	Med.	75^{th} perc.
Ersa	1.4×10^{-1}	1.6×10^{-1}	3.0×10^{-1}	6.6	7.1	12.2	3.3×10^{-3}	4.1×10^{-3}	4.6×10^{-3}
Finokalia	1.9×10^{-1}	2.6×10^{-1}	2.8×10^{-1}	10.4	16.7	25.6	3.4×10^{-3}	6.2×10^{-3}	9.3×10^{-3}

Table 3 Average growth rates and formation rates computed for the three case studies at Ersa and Cap Es Pinar.

	Ersa		Cap Es Pinar	
	GR_{15-25} (nm h^{-1})	J_{20} (cm^{-3} s^{-1})	GR_{15-25} (nm h^{-1})	J_{20} (cm^{-3} s^{-1})
July 5^{th}	16.4	2.4×10^{-1}	7.8	4.1×10^{-2}
July 29^{th}	8.9	7.9×10^{-2}	4.8	7.8×10^{-2}
August 9^{th}	4.3	4.8×10^{-2}	3.8	4.2×10^{-2}

Figures

Figure 1: Localization of the stations: Ersa (Corsica), Finokalia (Crete) and Cap Es Pinar (Mallorca). Aircraft flight paths from July 30th and August 1st are also shown.

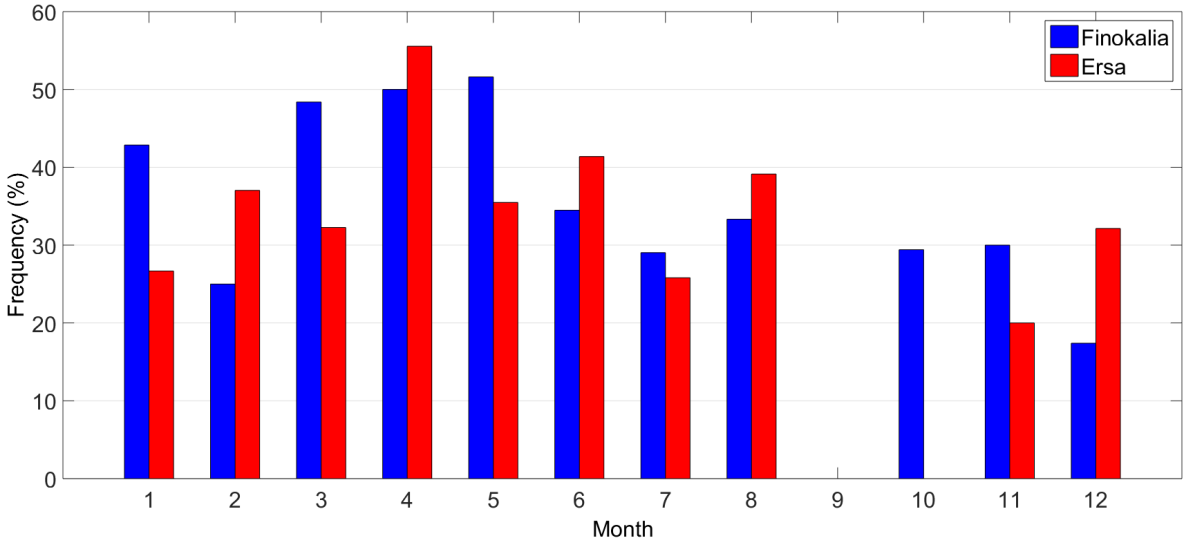

Figure 2: Monthly mean NPF frequencies at Finokalia and Ersa.

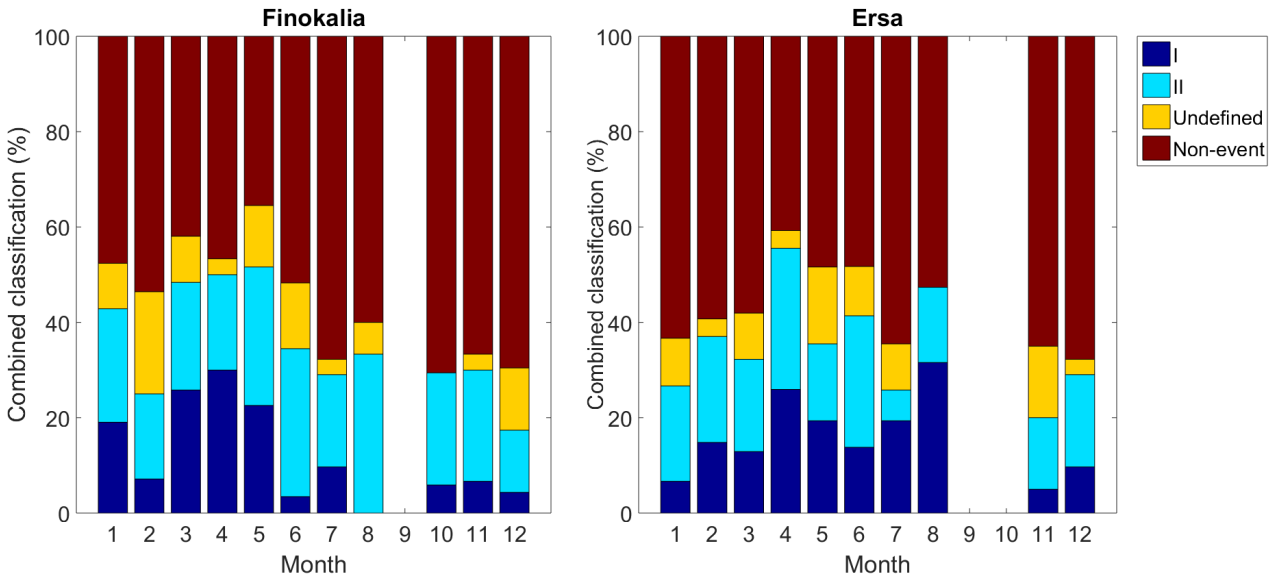

675 Figure 3: Monthly classification of the measurement days into event (I and II), undefined and non-
676 event categories in Finokalia and Ersa.

677

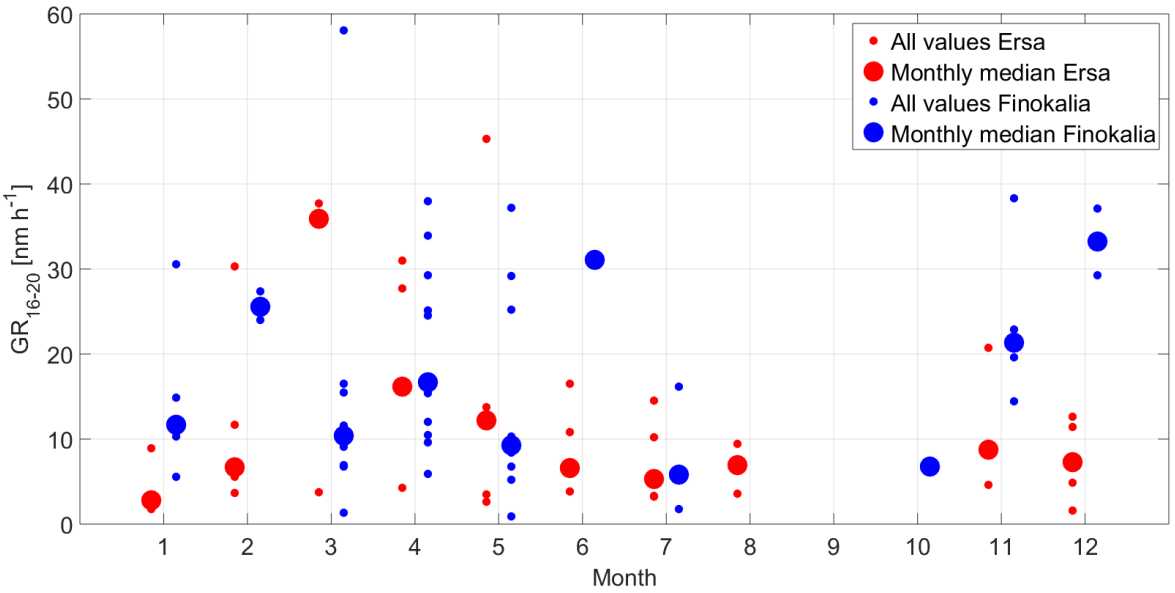

678

679 Figure 4: Annual variation of particle growth rate calculated for the range 16 – 20 nm at Ersa and for
680 type I events. Small dots represent all values while large dots stand for median values.

681

682

683

684

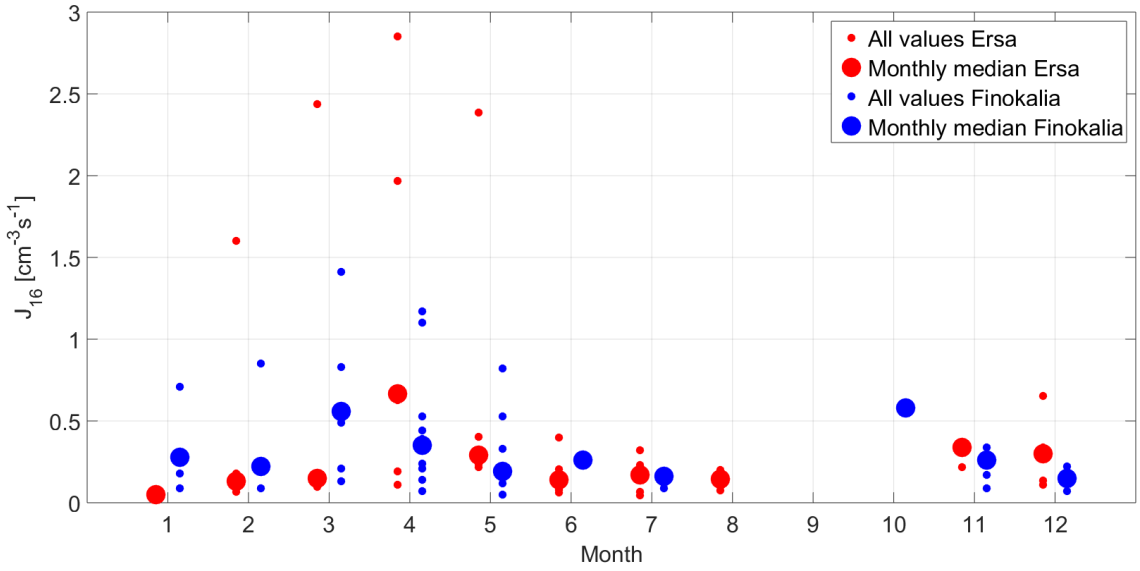

685

686 Figure 5: Annual variation of the 16 nm particle formation at Ersa and Finokalia for type I events.
687 Small dots represent all values while large dots stand for median values.

689

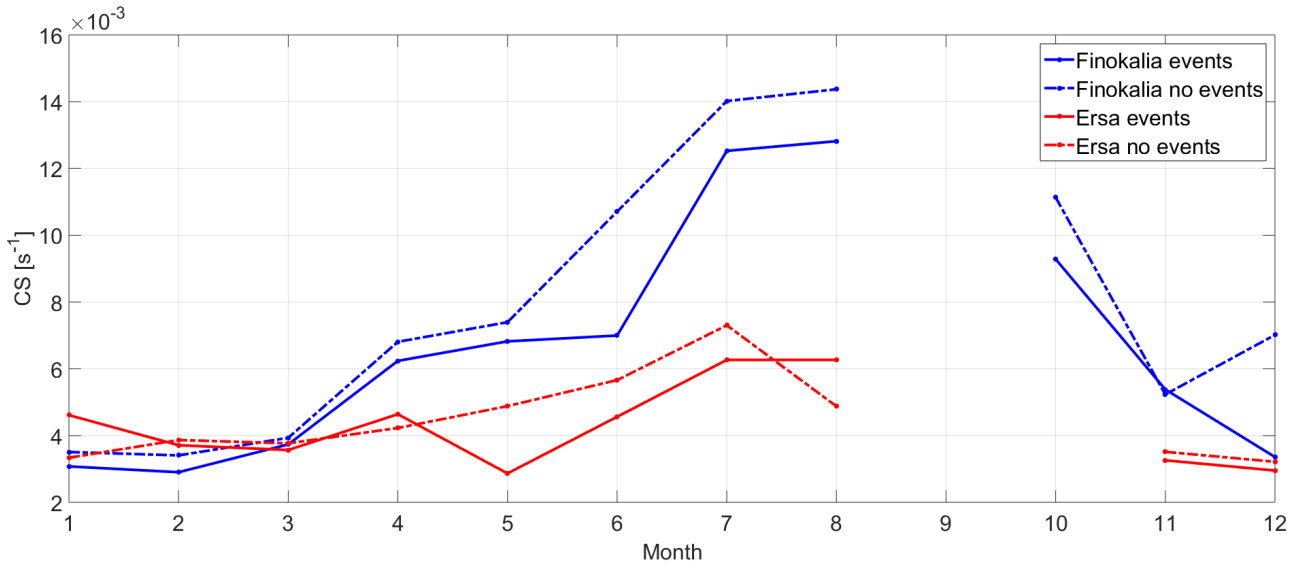

690

691 Figure 6: Median values of condensation sink (CS) reported separately for event and non-event days in
692 Finokalia and Ersa.

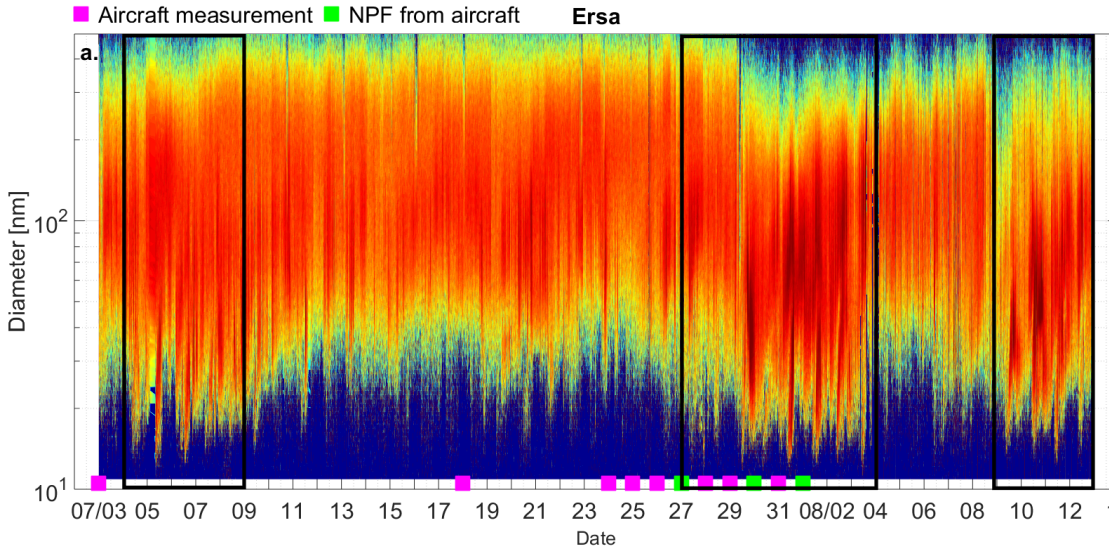
Aircraft measurement
NPF from aircraft
Ersa
a.
Diameter [nm]
10^2
10^1
07/03 05 07 09 11 13 15 17 19 21 23 25 27 29 31 08/02 04 06 08 10 12
Date

693

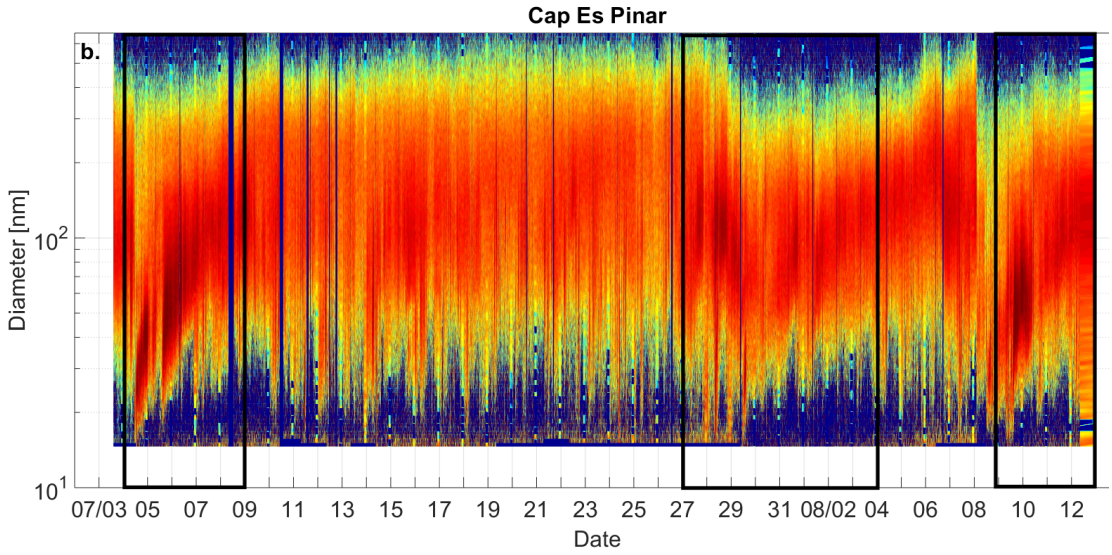
Cap Es Pinar
b.
Diameter [nm]
10^2
10^1
07/03 05 07 09 11 13 15 17 19 21 23 25 27 29 31 08/02 04 06 08 10 12
Date

694

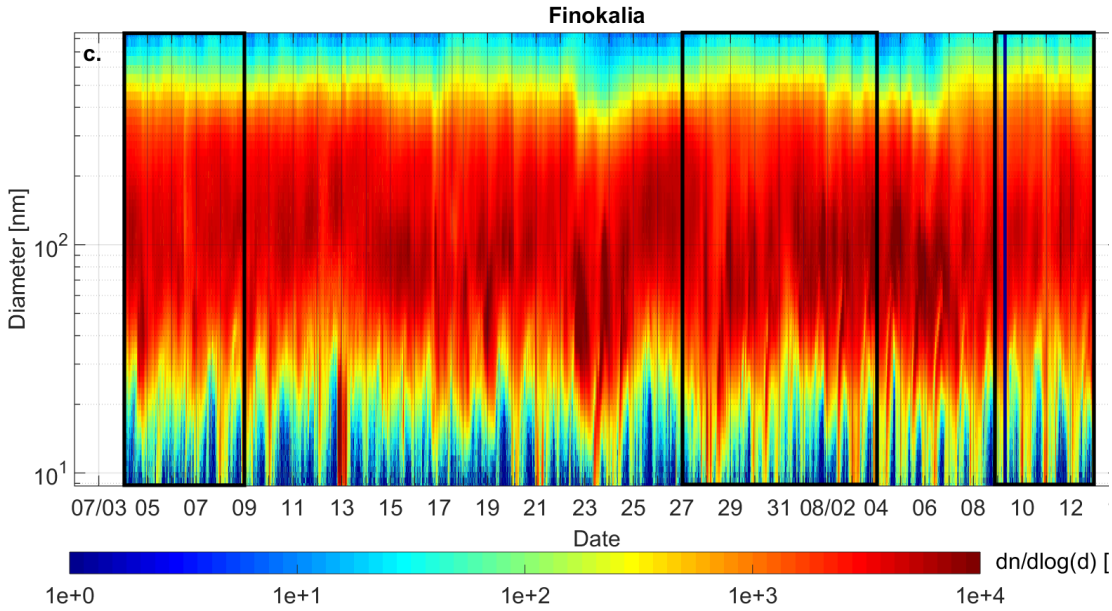
Finokalia
c.
Diameter [nm]
10^2
10^1
07/03 05 07 09 11 13 15 17 19 21 23 25 27 29 31 08/02 04 06 08 10 12
Date
dn/dlog(d) [
1e+0
1e+1
1e+2
1e+3
1e+4

695

Figure 7: SMPS particle number size distribution in a. Ersa, b. Cap Es Pinar and c. Finokalia during the SOP period. The three NPF episodes observed at large scale are highlighted on the spectra in the black boxes. The days of occurrence of the ATR-42 flights are also shown, together with the detection of NPF from these airborne measurements. Same color scale applies to a., b. and c..

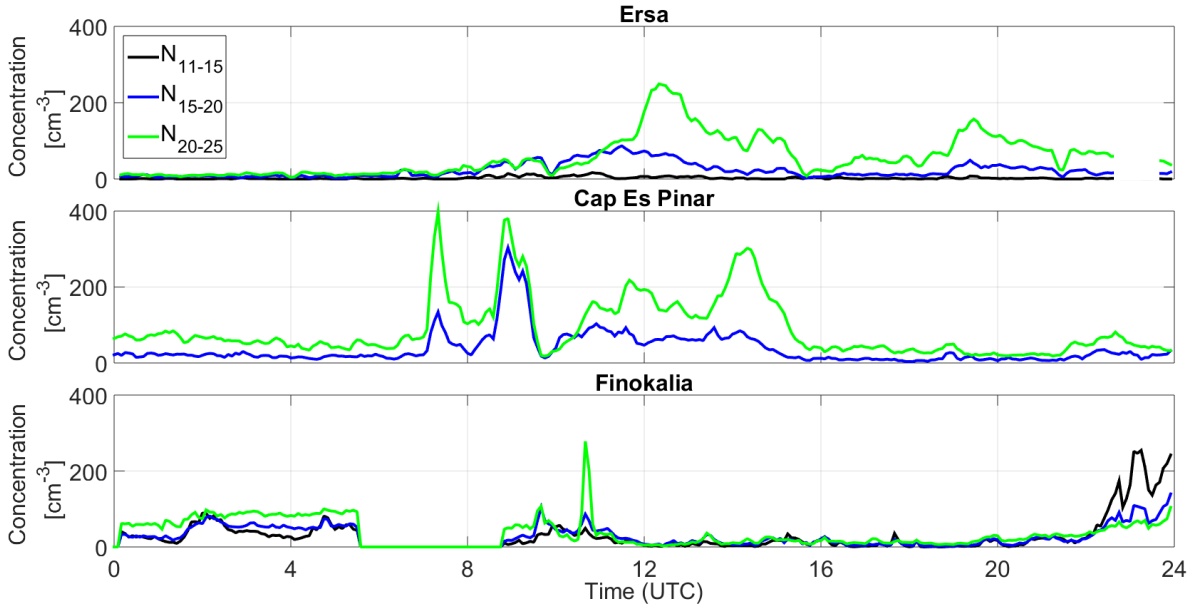

Figure 8: Temporal evolution of the particle concentrations in the size range 11-15 nm (black) (N_{11-15}), 15-20 nm (blue) (N_{15-20}) and 20-25 nm (green) (N_{20-25}) for August 9th event.

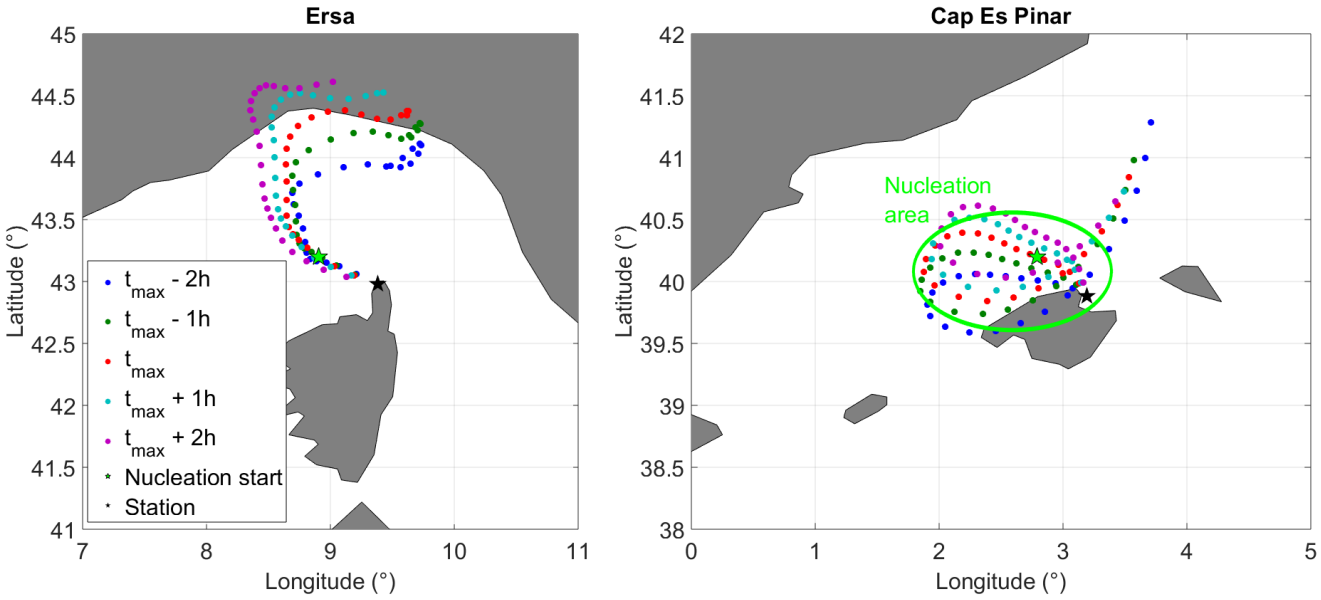

Figure 9: Back trajectories of air masses sampled in Ersa and Cap Es Pinar on August 9th at t_{max}, when 20 nm particles concentration is maximum, and during the two hours that precede and follow this

maximum. The location where nucleation initially occurs upstream the station is marked with a green star.

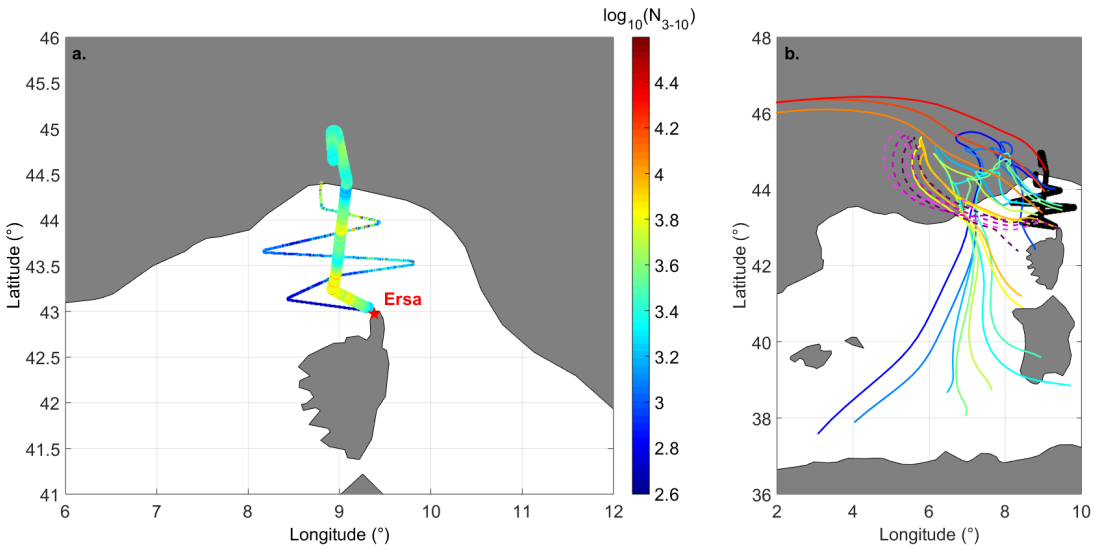

Figure 10: a. $N_{3\text{-}10}$ above the threshold value along the flight path performed on July 30th. Large size dots stand for high altitude measurements (~ 3400 m a.s.l.) while small size dots stand for low altitude measurements (~ 215 m a.s.l.); b. Air mass back trajectories calculated along the flight path (black line) every ten minutes (solid colored lines) together with the back trajectories of air masses arriving in Ersa each hour during the same time period (dashed lines).

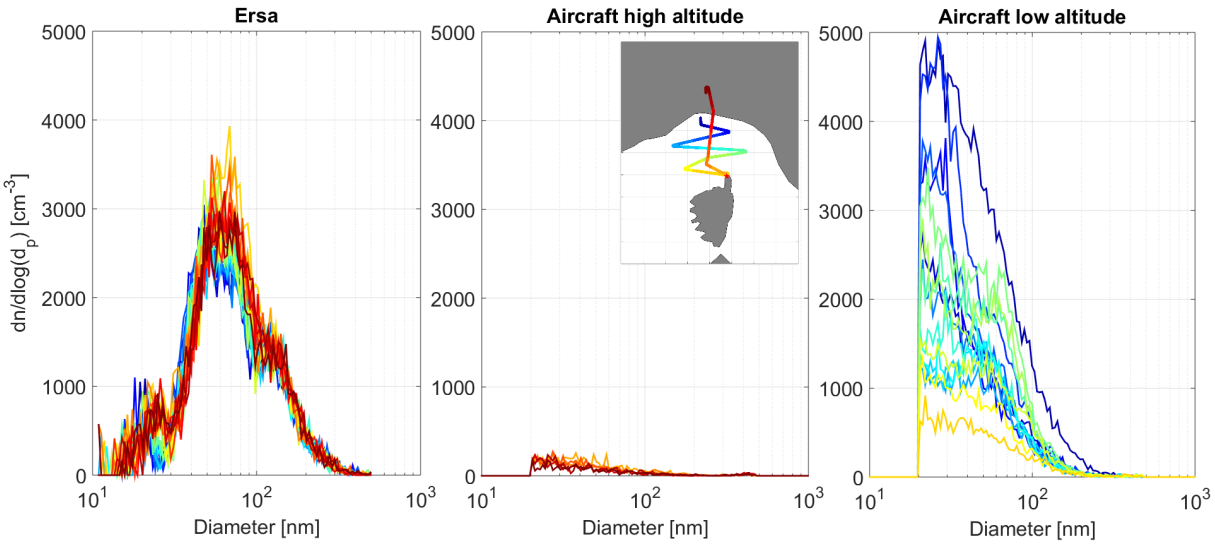

Figure 11: SMPS size distributions measured at Ersa (left panel) and onboard the ATR-42 at high altitude (~ 3400 m a.s.l.) (middle panel) and low altitude (~ 215 m a.s.l.) (right panel) on July 30th. The color coding of the size distributions corresponds to the location of the aircraft, as shown on the insert of the middle panel.

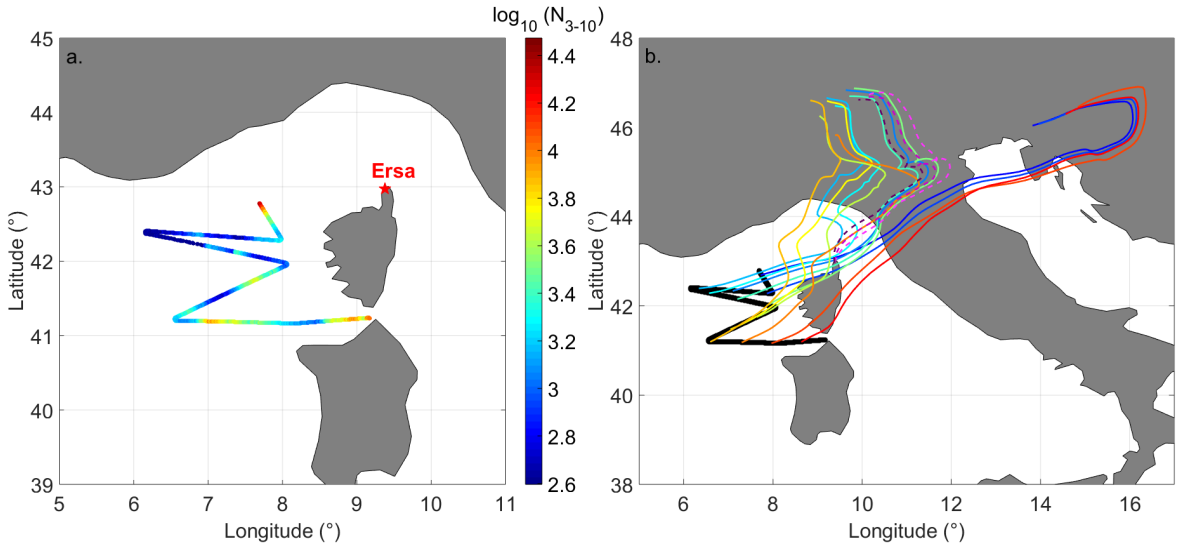

Figure 12: a. $N_{3\text{-}10}$ above the threshold value along the flight path; b. Air mass back trajectories (solid lines) calculated along the flight path (black line) every ten minutes (solid colored lines) together with the back trajectories of air masses arriving in Ersa each hour during the same time period (dashed lines) during the August 1st flight.

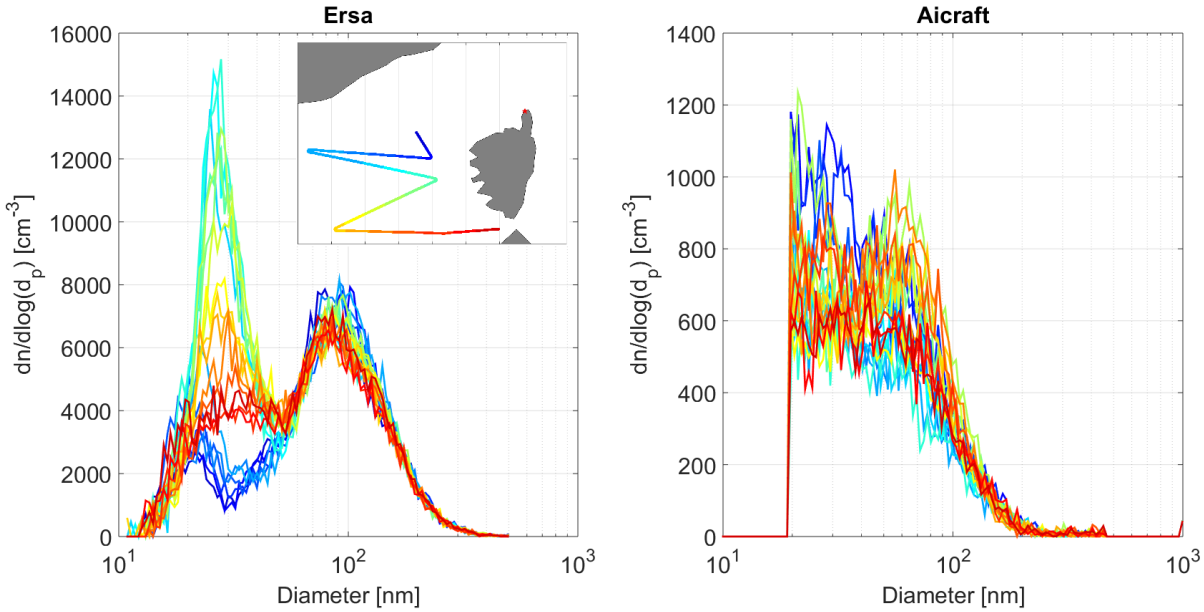

Figure 13: Ground based (left panel) and airborne (right panel) SMPS size distributions measured on August 1st . The color coding of the spectra corresponds to the location of the aircraft, as shown on the insert of the left panel.

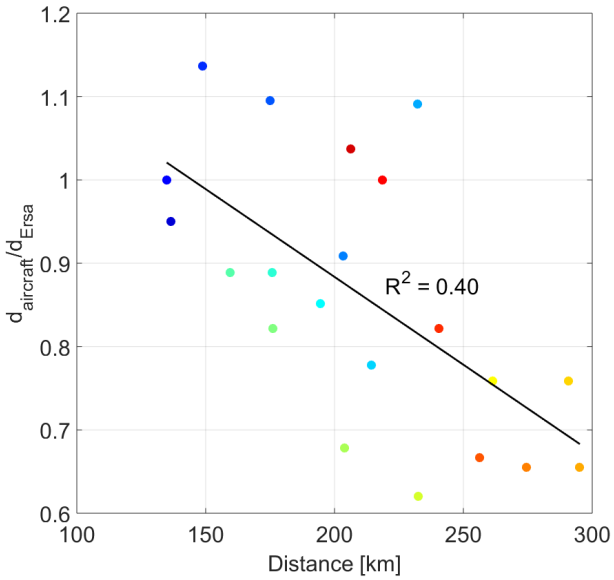

Figure 14: Ratio of nucleation mode diameters measured onboard the ATR-42 over that calculated in Ersa as a function of the distance between the aircraft and Ersa on August 1st. The color coding of this scatter plot matches with the location of the aircraft showed on the insert of the left panel of Figure 13.